

Abemaciclib induces atypical cell death in cancer cells characterized by formation of cytoplasmic vacuoles derived from lysosomes

Hirotsugu Hino^{1,2}  | Noriyoshi Iriyama³ | Hiroko Kokuba⁴ | Hiromi Kazama¹ | Shota Moriya¹ | Naoharu Takano¹ | Masaki Hiramoto¹ | Shin Aizawa² | Keisuke Miyazawa¹ 

¹Department of Biochemistry, Tokyo Medical University, Tokyo, Japan

²Division of Anatomical Science, Department of Functional Morphology, Nihon University School of Medicine, Tokyo, Japan

³Division of Hematology and Rheumatology, Department of Medicine, Nihon University School of Medicine, Tokyo, Japan

⁴Joint Research Center for Basic Medical Science, Tokyo Medical University, Tokyo, Japan

Correspondence

Keisuke Miyazawa, Department of Biochemistry, Tokyo Medical University, 6-1-1 Shinjuku, Shinjuku-ku, Tokyo 160-8402, Japan.

Email: miyazawa@tokyo-med.ac.jp

Funding information

Japan Society for the Promotion of Science, Grant/Award Number: JP18K15031; The Ministry of Education, Culture, Sports, Science and Technology of Japan, Grant/Award Number: S1411011

Abstract

In the cell cycle, the G₁/S transition is controlled by the cyclin-dependent kinase (CDK) 4/6-cyclin D complex. Constitutive activation of CDK4/6 dysregulates G₁/S transition, leading to oncogenic transformation. We found that 3 CDK4/6 inhibitors, abemaciclib, ribociclib, and palbociclib, exerted a cytotoxic effect as well as a cytostatic effect at the G₁ phase in cancer cell lines, including A549 human non-small cell lung cancer cells. Among these inhibitors, abemaciclib exhibited the most potent cytotoxic effect. The cell-death phenotype induced by abemaciclib, which entailed formation of multiple cytoplasmic vacuoles, was not consistent with apoptosis or necroptosis. Abemaciclib blocked autophagic flux, resulting in accumulation of autophagosomes, however vacuole formation and cell death induced by abemaciclib were independent of autophagy. In addition, methuosis, a cell-death phenotype characterized by vacuole formation induced by excessive macropinocytosis, was excluded because the vacuoles did not incorporate fluorescent dextran. Of note, both formation of vacuoles and induction of cell death in response to abemaciclib were inhibited by vacuolar-type ATPase (V-ATPase) inhibitors such as bafilomycin A1 and concanamycin A. Live-cell imaging revealed that the abemaciclib-induced vacuoles were derived from lysosomes that expanded following acidification. Transmission electron microscopy revealed that these vacuoles contained undigested debris and remnants of organelles. Cycloheximide chase assay revealed that lysosomal turnover was blocked by abemaciclib. Furthermore, mTORC1 inhibition along with partial lysosomal membrane permeabilization occurred after abemaciclib treatment. Together, these results indicate that, in cancer cells, abemaciclib induces a unique form of cell death accompanied by swollen and dysfunctional lysosomes.

KEYWORDS

abemaciclib, CDK4/6 inhibitor, lysosome, vacuole formation, V-ATPase

This is an open access article under the terms of the Creative Commons Attribution-NonCommercial License, which permits use, distribution and reproduction in any medium, provided the original work is properly cited and is not used for commercial purposes.

© 2020 The Authors. *Cancer Science* published by John Wiley & Sons Australia, Ltd on behalf of Japanese Cancer Association.

1 | INTRODUCTION

The cell cycle is precisely controlled by cyclin-dependent kinases (CDKs) whose activities are regulated by interactions with the corresponding cyclin proteins. At the G_1/S transition in normal cells, cyclin D is induced by mitogenic stimuli to form the CDK4/6-cyclin D complex. This complex is transported to the nucleus, where it phosphorylates retinoblastoma (Rb) protein. This leads to release of the sequestered transcription factor E2F from Rb and activates transcription of E2F-responsive genes required to drive the cell through the G_1/S transition.¹ Overexpression of cyclin D and CDK4/6, as well as constitutively active mutants of CDK4/6, has been detected in multiple types of human neoplasia.¹ Therefore, CDK4/6 is considered to be an important target for cancer therapy.²

The first CDK4/6-specific inhibitor, palbociclib (PD-0332991), was reported in 2004.^{3,4} Over the next decade, the next CDK4/6 specific inhibitors ribociclib (LEE011) and abemaciclib (LY-2835219) were developed,⁵⁻⁷ and many clinical trials have been performed for various neoplasia including non-small-cell lung cancer, colon cancer, and breast cancer.^{8,9} These inhibitors have been approved for breast cancer therapy by the FDA and the corresponding agencies in other countries.^{8,9} In terms of the therapeutic mechanism in cancer cells, these inhibitors block CDK4/6-cyclin D activity, leading to inhibition of Rb phosphorylation, which represses transcription of the genes associated with the G_1/S transition.¹⁰ Thus, these inhibitors are considered to induce a cytostatic effect, rather than a cytotoxic effect, in cancer cells.^{5,6} However, the precise molecular mechanism of the antitumor effect remains to be elucidated.

The lysosome is a cytoplasmic organelle that constitutes the primary digestive compartment of the cell and plays important roles in endocytosis, phagocytosis, and autophagy.¹¹⁻¹³ The luminal side of the lysosome maintains an acidic environment via the action of the vacuolar-type ATPase (V-ATPase), which functions as a proton pump across the lysosomal membrane. The lysosome contains more than 50 types of acid hydrolases including proteases, peptidases, nucleases, glycosidases, and lipases, which collectively are capable of digesting all types of macromolecules.^{14,15} Disorders of lysosomal activities caused by defects in these enzymes or V-ATPase component(s) induce many types of diseases, including lysosomal storage diseases, atherosclerosis, and Alzheimer's disease.^{14,16-19} In addition, the lysosome drives the progression of many types of human cancers through nutrient sensing by the lysosomal mTORC1 complex and nutrient scavenging by the autophagy system.²⁰⁻²³

In this study, we found that all 3 CDK4/6 inhibitors exert a cytotoxic effect in cancer cell lines. Among them, abemaciclib exhibited the most potent cytotoxic effect and also induced a form of cell death whose phenotypic characteristics were not consistent with apoptosis, necroptosis, autophagic cell death, or methuosis. Instead, the dying cells formed multiple large cytoplasmic vacuoles derived from expanded lysosomes. Because inhibitors of the V-ATPase almost completely inhibited vacuole formation, as well as repressing the cytotoxic effect, we conclude that abemaciclib induces a novel type of cell death characterized by formation of cytoplasmic vacuoles.

2 | MATERIALS AND METHODS

Cancer cell lines including the lung cancer cell line A549 and the breast cancer cell line MCF7 were cultured with abemaciclib, ribociclib, and palbociclib. Cytotoxic effect and cell-death phenotype induced by these CDK4/6 inhibitors were examined by cell viability assay, cytotoxicity assay, cell morphology, cell-cycle analysis, western blot analysis, autophagy flux assay, live-cell imaging, immunofluorescent staining, and transmission electron microscopy. The details are shown in Appendix S1.

3 | RESULTS

3.1 | Effects of CDK4/6 inhibitors on cell proliferation in A549 and MCF7 cells

We first investigated the effect of CDK4/6 inhibitors on the CDK4/6 activity and the cell growth of the lung cancer cell line A549 and the breast cancer cell line MCF7. The phosphorylation state of Rb, which is one of the critical substrates of CDK4/6, was reduced in A549 cells treated with these CDK4/6 inhibitors (Figure S1). A reduction in viable cell number was observed within 24 h in the presence of these inhibitors at concentrations on the order of 10-100 $\mu\text{mol/L}$ (Figure 1A-D). Similar dose-responses were seen in the cytotoxicity determined with lactate dehydrogenase (LDH) release assay (Figure 1E-H) and propidium iodide (PI) staining assay (Figure S2). In addition, the timing of cell death induced by these inhibitors became early in a dose-dependent manner (Figure S2). Among the 3 CDK4/6 inhibitors, abemaciclib was the most potent growth inhibitor (Figure 1A-D, Table S1). Cell-cycle analysis revealed that these cells were partially arrested at the G_1 phase after exposure to abemaciclib (control vs abemaciclib; $63.1 \pm 2.77\%$ vs $73.1 \pm 3.47\%$ at 24 h, $66.0 \pm 2.20\%$ vs $73.7 \pm 2.28\%$ at 48 h in A549, 51.13 ± 1.85 vs 55.72 ± 0.30 at 24 h, 52.33 ± 2.36 vs 61.14 ± 4.99 at 48 h in MCF7) (Figure 1I-L). These results indicate that cell growth inhibition by these CDK4/6 inhibitors was due to not only a cytostatic effect but also a cytotoxic effect.

3.2 | Abemaciclib-induced atypical cell death accompanied by cytoplasmic vacuole formation

To analyze the cell-death phenotype, we next examined the morphological changes after treatment with CDK4/6 inhibitors at concentrations around the IC_{50} for 24 h (Table S1). Many large cytoplasmic vacuoles were observed in A549 cells within 24 h of abemaciclib treatment (Figure 2A). Palbociclib induced smaller and fewer cytoplasmic vacuoles than abemaciclib, whereas ribociclib caused no vacuole formation (Figure 2A). Although abemaciclib induced cell death, neither adherent nor detached A549 cells contained nuclear fragments, chromatin condensation, or apoptotic bodies, all of which are characteristic features of cells undergoing apoptosis (Figure 2A,B).

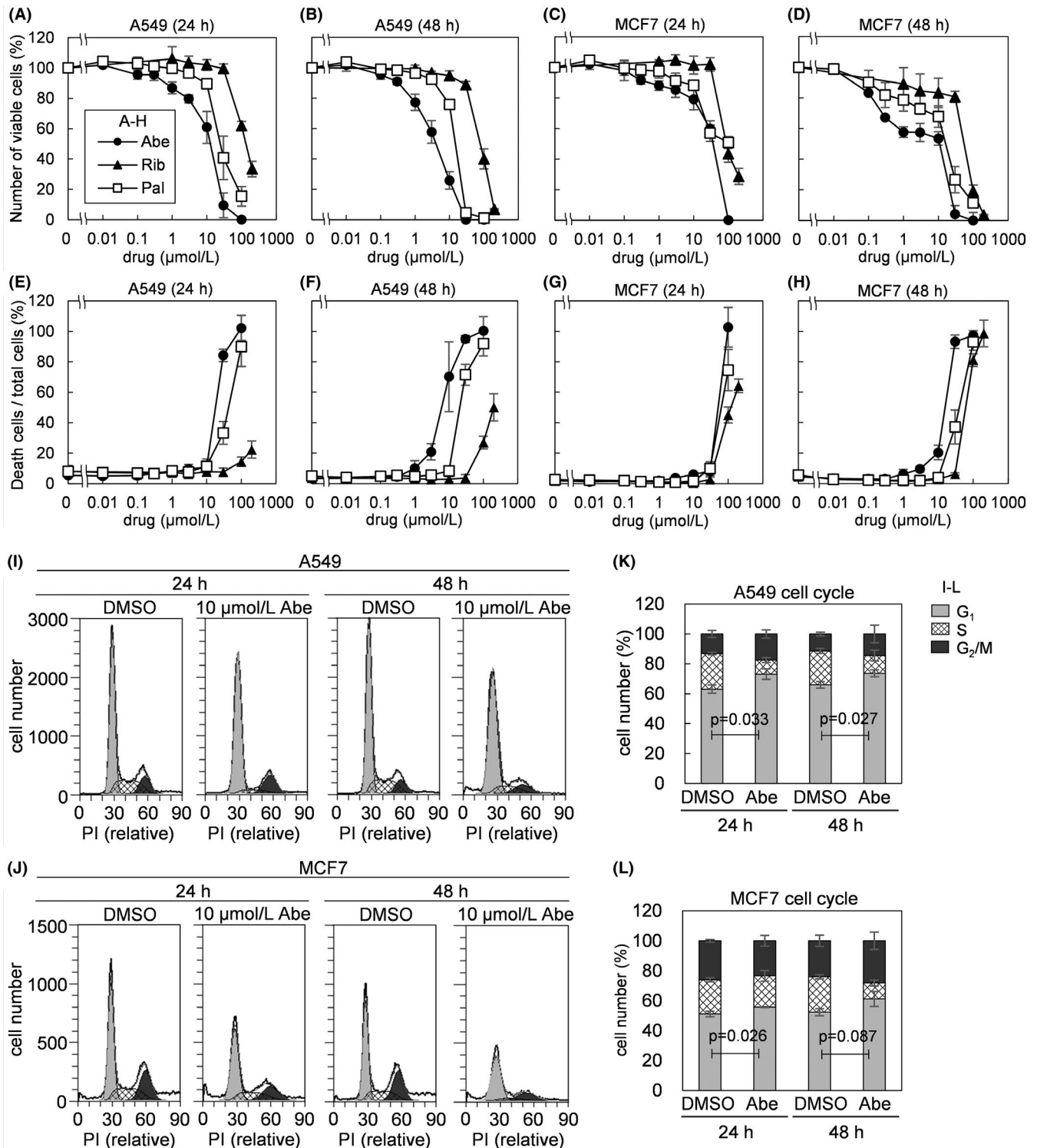


FIGURE 1 Effects of CDK4/6 inhibitors on proliferation of A549 and MCF7 cells. A-D, A549 and MCF7 cells were treated with abemaciclib (Abe), ribociclib (Rib), or palbociclib (Pal) at indicated concentrations for 24 or 48 h. Cell viability was analyzed, and the number of viable cells cultured in control medium was defined as 100%. Data represent average values from 3 independent experiments. E-H, A549 and MCF7 were treated with same conditions as in A-D. Cytotoxicity was analyzed, and the number of total cells (viable and death cells) counted in each condition was defined as 100%. I-L, A549 and MCF7 cells were treated with the indicated concentrations of Abe for 24 or 48 h. After fixation, cells were stained with PI, and the cell-cycle profile was analyzed by flow cytometry using the ModFit LT 5.0 software. Representative data are shown (I, J). Data represent average values from 3 independent experiments and *P*-values of *t* tests are indicated (K, L)

Similar morphological changes were observed in MCF7, CAL 27, and HT-29 cells (Figure S3), suggesting that abemaciclib induces non-apoptotic cell death. Western blotting for proteins involved in induction of cell death revealed that, in abemaciclib-treated A549 cells, poly(ADP-ribose) polymerase (PARP) was cleaved but caspase-3 was not cleaved much, indicating that the contribution of apoptosis to the observed cell death was scarce (Figure 2C). In addition, we detected no phosphorylation of receptor interacting protein 1 kinase 1 (RIPK1) and mixed lineage kinase domain-like (MLKL) as determined using phosphorylation-specific antibodies, and no phosphorylation of RIPK3 as determined by mobility shift in acrylamide gel; the phosphorylated states of these proteins indicate cells undergoing necroptosis²⁴⁻²⁷ (Figure 2C). In A549 cells, abemaciclib-induced cell death was partially rescued with small significant difference to control in the presence of either the pan-caspase inhibitor Z-VAD-fmk or the necroptosis inhibitor necrostatin-1 (Figure 2D top). These observations suggest that apoptosis and necroptosis make very minor contributions to abemaciclib-induced cell death. Moreover, in contrast to thapsigargin treatment, a well known inducer of endoplasmic reticulum (ER) stress, there was no induction of the ER stress-related pro-apoptotic transcription factor CCAAT-enhancer-binding protein homologous protein (CHOP)/GADD153 (Figure 2C).²⁸ This also suggests that induction of cell death by abemaciclib was not mediated through ER stress loading. Additionally, *N*-acetyl-L-cysteine, a reactive oxygen species (ROS) scavenger, had modest effect with significant difference to control abemaciclib-induced cell death (Figure 2D bottom), suggesting that ROS did not play a major role in induction of cell death. Taken together, these data suggest that the cell-death phenotype induced by abemaciclib does not correspond to apoptosis and necroptosis.

3.3 | CDK4/6 inhibitors suppress autophagic flux

It was reported that CDK4/6 inhibitors induce autophagy.²⁹⁻³⁵ Based on the results described above, we speculated that the prominent vacuole formation in response to abemaciclib might be related to autophagy. Western blotting revealed that microtubule-associated protein light chain 3 (LC3B)-II, a marker of autophagosomes, increased during a 1-24-h exposure to these inhibitors at concentrations near their IC_{50} in A549 cells (Figures 3A,B and S4A,B), and p62/SQSTM1 increased during a 1-24-h exposure to abemaciclib and ribociclib (Figures 3A,B and S4A,B). In addition, we performed autophagic flux assays using GFP-LC3-mCherry-LC3 Δ G probes in A549 cells.³⁶ In this system, the probe is cleaved by endogenous ATG4 protease and produces the same amount of GFP-LC3 and mCherry-LC3 Δ G. GFP-LC3 is involved in autophagosome membrane formation via conjugation of phosphatidylethanolamine at the C-terminal glycine residue. Subsequently, GFP-LC3 is bleached and degraded by lysosomal hydrolases in an acidic environment via autolysosome formation during autophagic processing. In contrast to GFP-LC3, mCherry-LC3 Δ G derived from the probe lacks the glycine residue

and remains in the cytosol, serving as an internal control because it is exempt from lysosomal degradation. Therefore, autophagic flux can be monitored by the GFP/mCherry signal ratio.³⁷ When the cells were cultured in HBSS, a starvation condition that induces autophagy, the GFP/mCherry ratio was indeed lower than in cells cultured in control medium whereas, in the presence of bafilomycin A1, a well known inhibitor of autophagy, the ratio was elevated. In addition, when autophagic flux was blocked by bafilomycin A1, prominent GFP-LC3 dots (representing autophagosome accumulation) were detected, confirming the ability of this assay system to monitor autophagic flux (Figure 3C,D). As shown in Figure 3C, treatment with abemaciclib and ribociclib increased the GFP/mCherry ratio, indicating inhibition of autophagic flux. Consistent with this, both drugs caused accumulation of GFP-LC3 dots, as in the case of bafilomycin A1 treatment (Figures 3D and S4C). The GFP/mCherry ratio exhibited a biphasic curve over a 24-h treatment period with palbociclib, which exerted a weaker effect on autophagy than abemaciclib (Figure 3C). Collectively, these results indicate that CDK4/6 inhibitors suppress autophagic flux in A549 cells. In addition, when we compared blocking of autophagic flux among the 3 CDK4/6 inhibitors at concentrations near the IC_{50} for cell growth, abemaciclib had the most prominent effect, as it did on formation of cytoplasmic vacuoles.

3.4 | Abemaciclib-induced cell death and vacuole formation are suppressed by V-ATPase inhibitors but independent of autophagy

To examine the relationship between abemaciclib-induced cell death and autophagy, we examined the effects of autophagy inhibitors on abemaciclib-induced cell death using 3-methyladenine, an inhibitor of class III PI3K, and bafilomycin A1 and concanamycin A, both of which are inhibitors of V-ATPase. Abemaciclib-induced cell death was rescued in the presence of bafilomycin A1 or concanamycin A (Figure 4A center and right), but not 3-methyladenine (Figure 4A left). In addition, we established ATG5-KO A549 cells. ATG5 is essential for modification of LC3B with phosphatidylethanolamine to form LC3B-II, which is involved in autophagosome membrane formation. Consequently, ATG5-KO cells are deficient in autophagy (Figure 4B). In these cells, abemaciclib still induced cell death that was attenuated by bafilomycin A1, as in control KO cells (Figure 4C). Moreover, abemaciclib-induced vacuole formation was almost completely inhibited in the presence of bafilomycin A1 or concanamycin A (Figure 4D,E). Furthermore, in ATG5-KO cells, abemaciclib induced vacuole formation, which was suppressed by bafilomycin A1 as in control KO cells (Figure S5). These results indicate that vacuole formation is independent of autophagy. Taken together, these results indicate that the cell-death phenotype induced by abemaciclib does not represent "autophagic cell death," a cell death phenotype characterized by excessive induction of autophagy.³⁸ In addition, because bafilomycin A1 and concanamycin A, but not 3-methyladenine,

FIGURE 2 Analysis of the cell-death phenotype induced by abemaciclib. A, A549 cells were treated with Abe, Rib, or Pal for 24 h. After fixation, adherent cells on a cover glass were stained with May-Grünwald-Giemsa. B, A549 cells were treated with the indicated concentrations of Abe for 24 h. Detached and adherent cells were spread together on glass slides, and subsequently stained with May-Grünwald-Giemsa. Scale bars in A and B: 20 μ m. C, A549 cells were treated with the indicated concentrations of Abe for 10 or 24 h. Cellular proteins were extracted and analyzed by western blotting using the indicated antibodies. "P-" means "phosphorylated." As a positive control for apoptosis, CAL 27 cells were treated with 1 μ mol/L staurosporine for 4 h. As a positive control for necroptosis, HT-29 cells were pretreated with 20 μ mol/L Z-VAD-fmk for 1 h, and subsequently treated with 10 μ g/mL CHX and 10 ng/mL tumor necrosis factor- α for 12 h (indicated as ZCT). As a positive control for ER stress, A549 cells were treated with 1 μ mol/L thapsigargin for 24 h. D, A549 cells were treated with the indicated concentrations of Abe with or without 50 μ mol/L Z-VAD-fmk, 50 μ mol/L necrostatin-1 (Nec-1), necrostatin-1 inactive control (IA-Nec-1), 10 mmol/L *N*-acetyl-L-cysteine (NAC). After a 24-h treatment, the viability was analyzed; the number of viable cells in samples treated with control medium containing the equivalent concentration of DMSO or buffer was defined at 100%. Data represent average values from 3 independent experiments. *P*-values of *t* tests are indicated

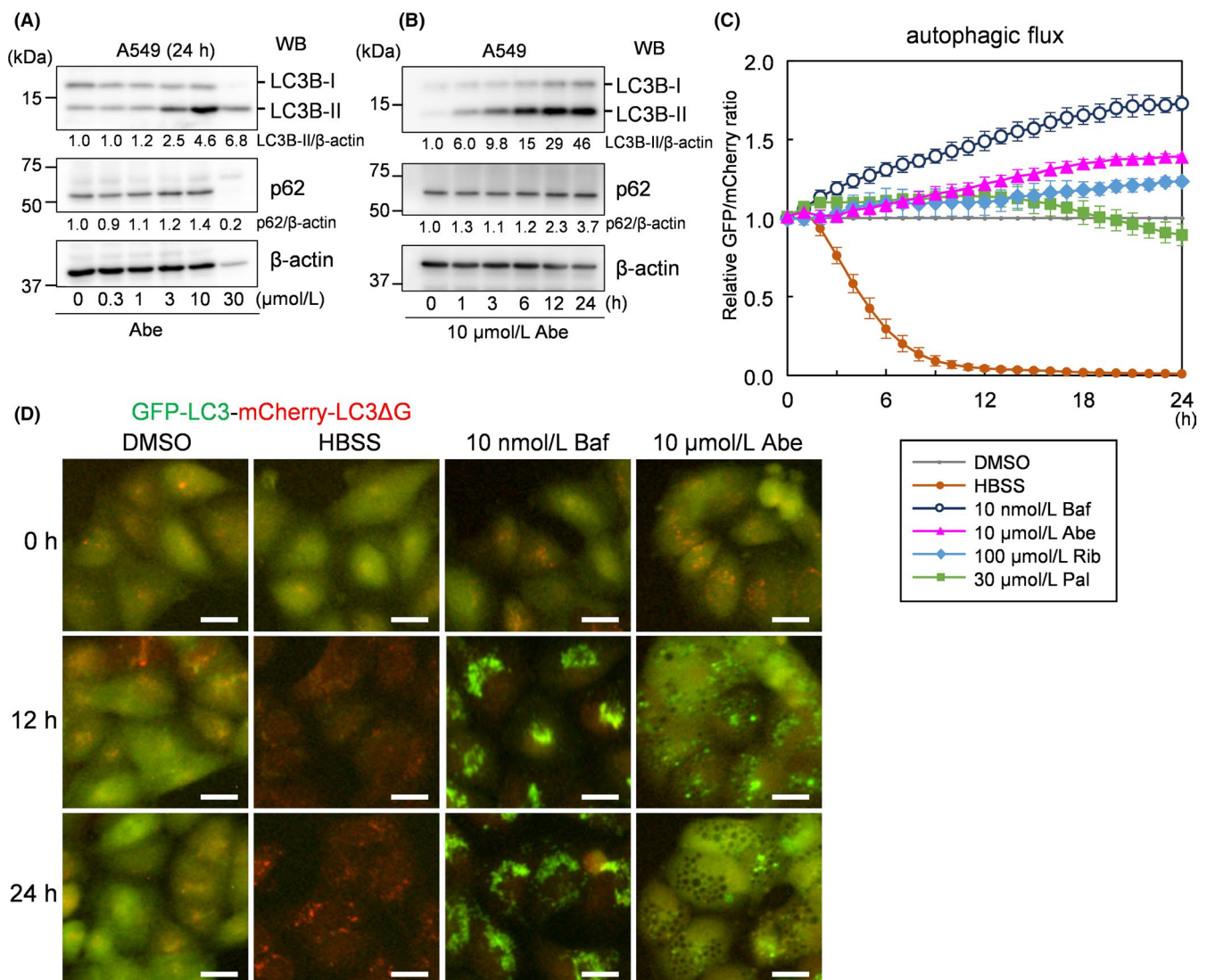


FIGURE 3 Effects of CDK4/6 inhibitors on autophagic flux. A, B, A549 cells were treated with Abe at the indicated concentration for 24 h (A) or the indicated time periods (B). Western blotting used the indicated antibodies. Signal intensity of each band was quantified using CS Analyzer 4 software (ATTO), normalized by β -actin, and is shown below. C, D, A549/GFP-LC3-mCherry-LC3 Δ G cells were cultured in the presence of the indicated reagents or culture medium, and fluorescence images were obtained on an IncuCyte ZOOM cell imaging system every hour over a 24-h culture (D, green and red merged images at 0, 12, or 24 h, the images of cells treated by Rib and Pal are shown in Figure S4C). The intensities of GFP-LC3 and mCherry-LC3 Δ G in each field were measured using the same cell imaging system. The ratio of the fluorescence intensities of GFP and mCherry was calculated and expressed relative to the value from control cells cultured in control medium containing 0.5% DMSO. Data represent average values from 3 independent experiments (C). Scale bars in D: 20 μ m

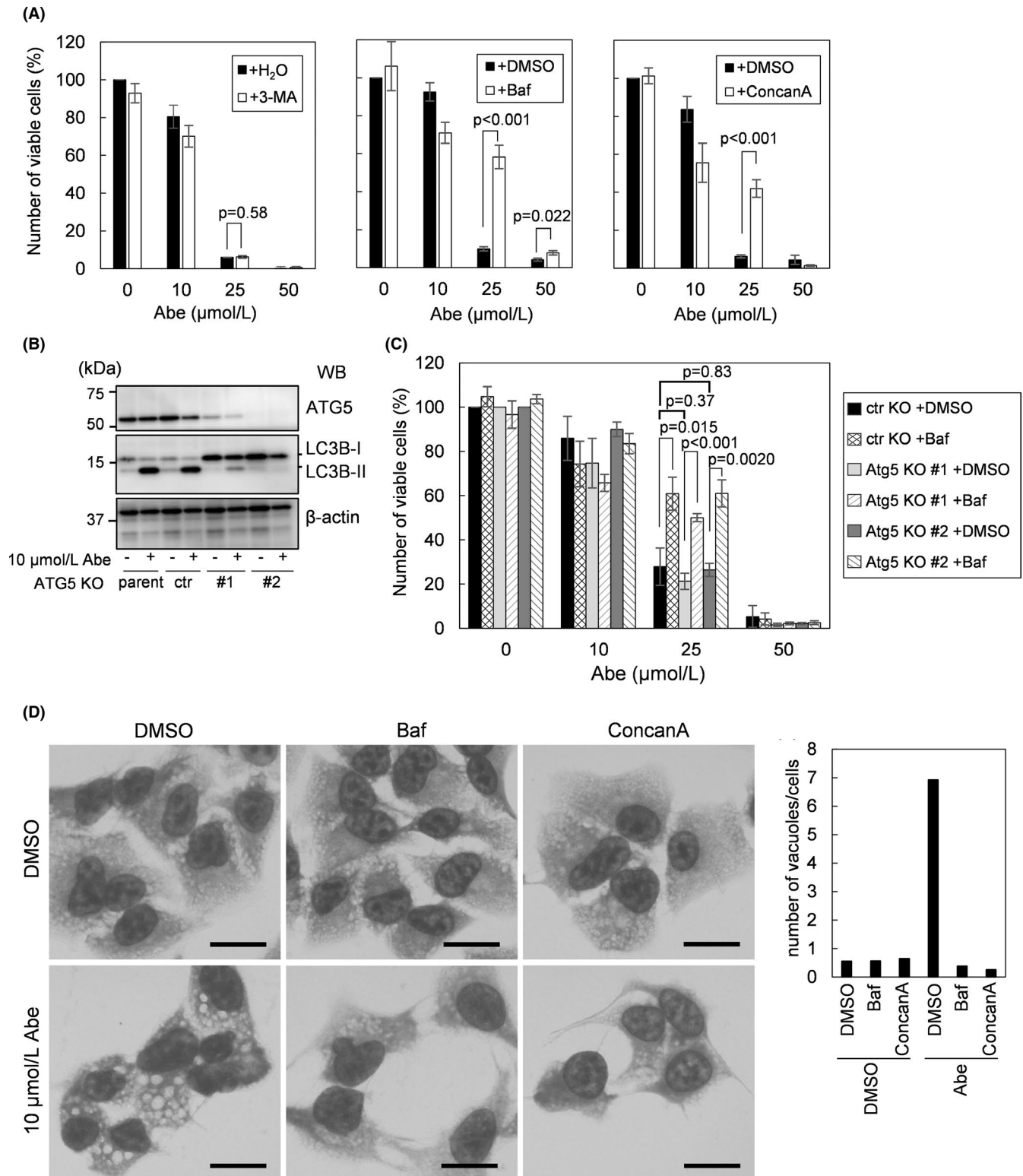


FIGURE 4 Inhibitory effects of V-ATPase inhibitors in abemaciclib-induced cell death and cytoplasmic vacuole formation. **A**, A549 cells were treated with the indicated concentrations of Abe with or without 3 nmol/L bafilomycin A1 (Baf), 1 nmol/L concanamycin A (ConcanA), or 1 mmol/L 3-methyladenine (3-MA). After a 24-h treatment, the viability was analyzed; the number of viable cells in samples treated with control medium containing the equivalent concentration of DMSO or water was defined as 100%. Data represent average values from 3 independent experiments. *P*-values of *t* tests are indicated. **B**, ATG5-KO A549 cells were treated with or without 10 $\mu\text{mol/L}$ Abe for 24 h, and subsequently analyzed by western blotting with the indicated antibodies. **C**, ATG5-KO A549 cells were treated with the indicated concentrations of Abe and/or 3 nmol/L Baf. Data represent average values from 3 independent experiments. *P*-values (*t* test) for +Baf vs -Baf samples are indicated above narrow lines, and *P*-values for KO vs WT are indicated above bold lines. **D**, A549 cells were treated with the combination of Abe and 3 nmol/L Baf or 1 nmol/L ConcanA for 24 h. After fixation, adherent cells were stained with May-Grünwald-Giemsa. Scale bars: 20 μm . **E**, Number of vacuoles per cells of **D** was counted

suppressed both cell death and vacuole formation by abemaciclib, we hypothesized that V-ATPase is involved in this phenomenon.

3.5 | Most of cytoplasmic vacuoles induced by abemaciclib are derived from expanded lysosomes

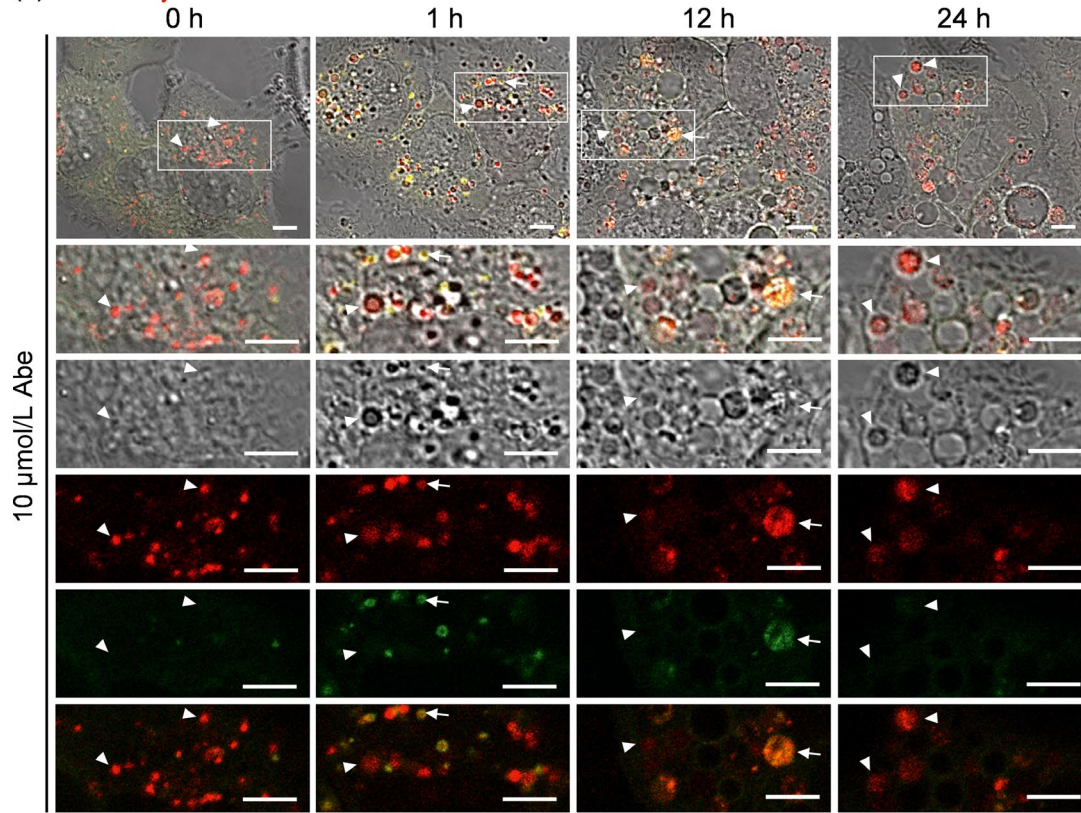
To investigate the origin of cytoplasmic vacuoles induced by abemaciclib, we performed time-lapse imaging of mCherry-GFP-LC3-expressing A549 cells treated with abemaciclib (Figures 5A and S6A, Movie S1). In this system, because GFP is sensitive to acidic conditions, whereas mCherry is not, only the red fluorescent signal of mCherry is detectable after fusion of autophagosomes with lysosomes to form autolysosomes. Before abemaciclib treatment, we observed small red dots, indicating the basal state of the autolysosome (Figure 5A). After a 1-h exposure to abemaciclib, many yellow dots derived from both GFP and mCherry (indicating autophagosomes) became detectable (Figure 5A, arrow), although most of them did not colocalize to vacuoles, and some small vacuoles contained mCherry red fluorescence only (indicating autolysosomes) (Figure 5A, indicated as arrowhead). Over time, as the vacuoles became larger and more numerous, only a subset contained the mCherry signal. Therefore, some but not all of the cytoplasmic vacuoles were derived from autolysosomes. As shown in Figure 4D,E, vacuole formation was suppressed by V-ATPase inhibitors, so we speculated that abemaciclib-induced vacuoles might be expanded lysosomes. To test this possibility, we next established an A549 cell line stably expressing lysosomal-associated membrane protein (LAMP1)-mCherry and performed time-lapse imaging over a 24-h exposure to abemaciclib (Figures 5B and S6B, Movies S2 and S3). In this assay, we also stained cells with LysoSensor Green DND-189, which detects lysosomal acidification. The pKa of this LysoSensor Green is ~5.2. Before treatment with abemaciclib, we observed many small red dots (LAMP1-mCherry) without green fluorescence (LysoSensor Green), suggesting that under basal conditions, the lysosomes were not acidic enough to stain with the acidification sensor. After 1 h of abemaciclib treatment, we observed some small vacuoles containing both LAMP1-mCherry and LysoSensor Green fluorescence (Figure 5B, indicated as arrow). Of note, most of the vacuoles became larger (Figure 5B,C), and most of them stained with LysoSensor Green, and contained marginal localization of LAMP1-mCherry; ultimately, some of the LysoSensor Green fluorescence disappeared (Figure 5B, indicated as arrowhead). These observations suggest that the swollen lysosomes became acidic and finally appeared to lose their function in response to abemaciclib treatment. At 12–24 h after abemaciclib treatment, a few vacuoles appeared in which neither LAMP1-mCherry nor LysoSensor Green was localized, suggesting that their origin was not lysosomes. In addition, to evaluate macropinocytosis,^{39–41} we assessed the uptake of fluorescent dextran into endosomes in the presence or absence of abemaciclib. In control cells, many green fluorescent dots caused by dextran uptake (indicating endosome) were observed and some of these dots colocalized to LAMP1-mCherry dots (indicating lysosome) (Figure

S6C). Conversely, in abemaciclib-treated cells, although fluorescent dextran dots were also observed, some of them were larger than that in control cells. Moreover, most fluorescent dextran did not co-localize with abemaciclib-induced vacuoles containing LAMP1-mCherry (Figure 6). This suggests that most abemaciclib-induced vacuoles are not derived from endosomes produced by macropinocytosis, indicating that abemaciclib-induced cell death is not equivalent to methuosis, which is a cell-death phenotype characterized by vacuole formation induced by excessive macropinocytosis.^{42–44}

3.6 | Abemaciclib induces lysosomal dysfunction which appears to be responsible for cell death execution

Finally, to investigate the mechanism of abemaciclib-induced cell death, we examined the effects of abemaciclib on lysosome function. Transmission electron microscopy revealed that, in addition to enlarging, the vacuoles became more abundant during a 24-h exposure to abemaciclib (Figure 7A). Most of these expanded vacuoles contained indigestible debris and remnants of organelles. This vacuolar “indigestion” persisted for at least 24 h during exposure to abemaciclib, supporting the idea that the vacuoles were derived from dysfunctional lysosomes (Figure 7A, lower panels). The mitochondria, ER, and nucleus were intact in abemaciclib-treated cells, indicating that the target of abemaciclib is lysosome rather than any of the other organelles. To analyze lysosomal turnover, we performed a cycloheximide (CHX) chase assay in the presence or absence of abemaciclib. When A549 cells were treated with CHX, lysosomal membrane proteins (LAMP1, 2) and proteasome-substrate protein (cyclin B) were degraded in a time-dependent manner (Figure 7B,C). However, when treating with CHX and abemaciclib, degradation of only lysosomal membrane proteins was blocked (Figure 7B,C), suggesting that abemaciclib disrupted lysosomal turnover. Next, to assess the lysosomal function as a platform for nutrient sensing and metabolic signal transduction through the mTORC1 protein kinase complex,^{20,45,46} we examined the mTORC1 activity in abemaciclib-treated cells. The level of phospho-mTOR kinase (active form of mTOR) and downstream effectors of mTORC1 signaling (phosphorylation of p70 S6 kinase and S6 ribosomal protein) were suppressed by abemaciclib treatment in a time-dependent manner (Figure 7D). This suggests that abemaciclib impairs the lysosomal function as a platform of mTORC1 signaling. Furthermore, we evaluated lysosomal membrane permeabilization (LMP) by observation of galectin-3 localization.⁴⁷ In nontreated cells, galectin-3 was diffused in cytosol (Figure S7A, top). As a positive control for LMP, treatment with L-leucyl-L-leucine methyl ester (LLOMe), a well known inducer for LMP, resulted in translocation and puncta formation of galectin-3 on the damaged lysosomes (containing LAMP2) (Figure S7A, bottom).^{47,48} After treatment with abemaciclib at 10 μmol/L for 24 h, galectin-3 puncta colocalized to lysosomes were observed in 32% of the cells. However, the number of galectin-3 puncta in abemaciclib-treated cells was lower than that in LLOMe-treated cells (Figure S7A

(A) mCherry-GFP-LC3



(B) LAMP1-mCherry+LysoSensor Green

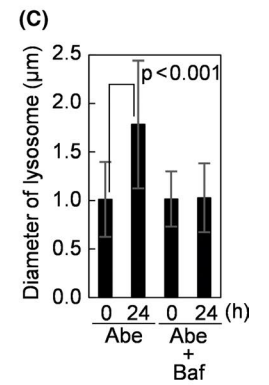
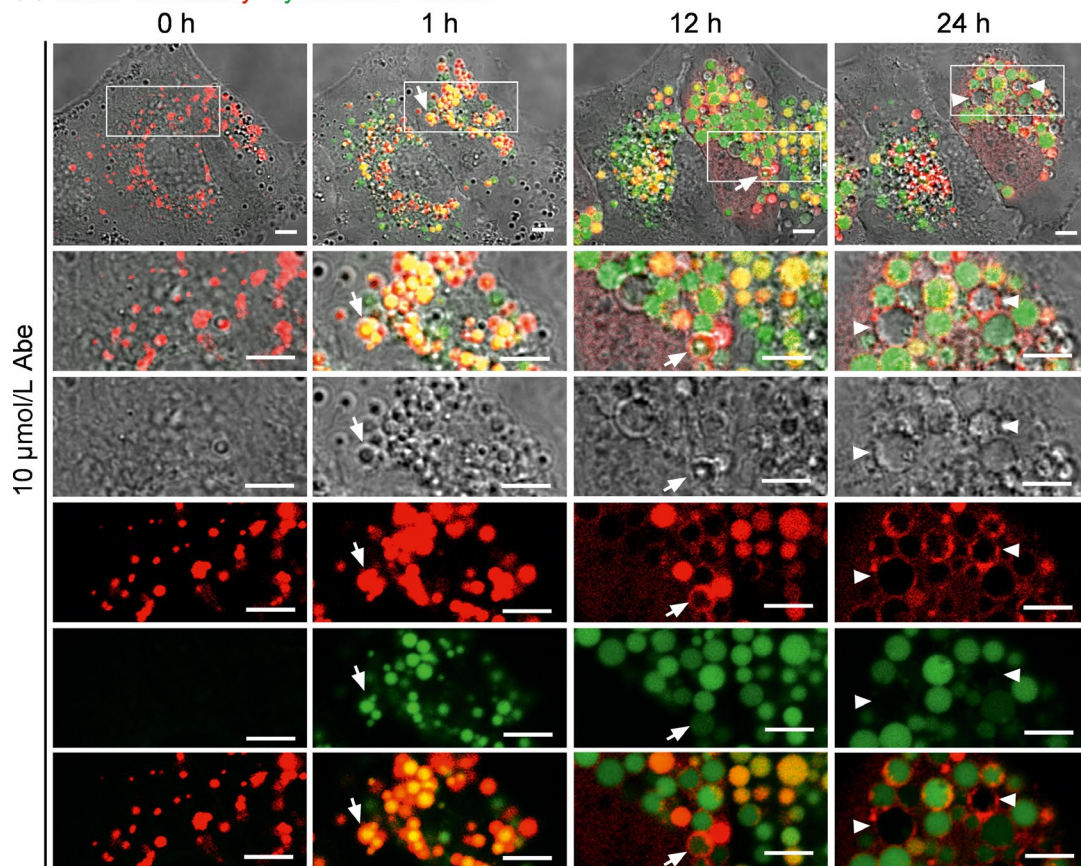


FIGURE 5 Analysis of cytoplasmic vacuole formation induced by abemaciclib. A, A549/mCherry-GFP-LC3 cells were treated with 10 $\mu\text{mol/L}$ Abe and subjected to time-lapse imaging. Merged fluorescence and bright-field images (top) are presented for each time point. Arrowheads indicate red vacuoles; arrows indicate yellow dots not colocalized to vacuoles. Bottom 5 line panels represent high-magnification images of the area indicated by open squares; merge, bright field, red (mCherry), green (GFP), and merge of red and green from the top. A movie generated from images collected at 10-min intervals is presented as Movie S1. B, A549/LAMP1-mCherry cells cultured with 200 nmol/L LysoSensor Green DND-189 were cultured in the presence or absence of 10 $\mu\text{mol/L}$ Abe and subjected to time-lapse imaging. Merged fluorescence and bright-field images (top) are presented for each time point. Arrows indicate vacuoles with red and green fluorescence, arrowheads indicate vacuoles with marginal red fluorescence alone. Bottom 5 lines panels represent high-magnification images of the area indicated by open squares; merge, bright field, red (LAMP1-mCherry), green (LysoSensor Green), and merge of red and green from the top. Movies generated from images of Abe-presence condition collected at 10-min intervals are presented as Movie S2 (merged with fluorescence and bright-field images) and Movie S3 (merged with red and green fluorescence images). In A and B, scale bars: 5 μm . The images not treated with Abe are presented as Figure S6A,B. C, The cells were cultured in the presence of Abe with or without 3 nmol/L Baf (shown in Figure 5B or not shown). Diameter of lysosome (green and yellow signal) in these cells at 0 or 24 h were quantitated using ImageJ software (1.50i, National Institutes of Health, USA). Data represent average values of at least 100 lysosomes. *P*-values of *t* tests are indicated

middle 2 lines, B). This suggested that LMP was modestly increased by abemaciclib. Additionally, an increase in intracellular calcium concentration, which has been reported to be increased in response to LMP,⁴⁹ was observed after 24 h treatment with abemaciclib (Figure S8A,B), although we could not detect a prominent increase of intracellular calcium concentration by 4 h treatment with LLOMe (Figure S8C,D). Taken together, our data suggest that abemaciclib treatment induces lysosomal dysfunction, concomitant with prominent lysosomal expansion and low levels of LMP, which appears to be responsible for cell-death execution.

4 | DISCUSSION

In this study, we revealed that abemaciclib induces atypical cell death associated with formation of cytoplasmic vacuoles derived from swollen lysosomes (Figures 1, 2, and 5); this effect was almost completely inhibited in the presence of V-ATPase inhibitors

(Figure 4D,E). Transmission electron microscopy revealed that these vacuoles contained undigested remnants of organelles (Figure 7A). Thus, abemaciclib might act directly or indirectly on V-ATPase, leading to lysosomal acidification via H^+ transport (Figure 5B). This effect on V-ATPase appears to induce lysosomal swelling via influx of H_2O , as well as lysosomal dysfunction followed by LMP and an increase of intracellular calcium concentration (Figures 7, S7, and S8, summarized in Figure 8). Because V-ATPase inhibitors also inhibited the cytotoxic effect of abemaciclib (Figure 4), loss of lysosomal integrity appeared to be closely related to the cytotoxicity of abemaciclib.

The phenotype we observed is superficially similar to methuosis, a form of cell death characterized by formation of multiple cytoplasmic vacuoles derived from endosomes via facilitation of macropinocytosis.⁴²⁻⁴⁴ However, fluorescent dextran taken up into endosomes via macropinocytosis did not extensively co-localize with most of the abemaciclib-induced vacuoles containing LAMP1-mCherry (Figures 6 and S6C), indicating that cell-death phenotype induced by abemaciclib is distinct from methuosis. Recently, LMP has come to be

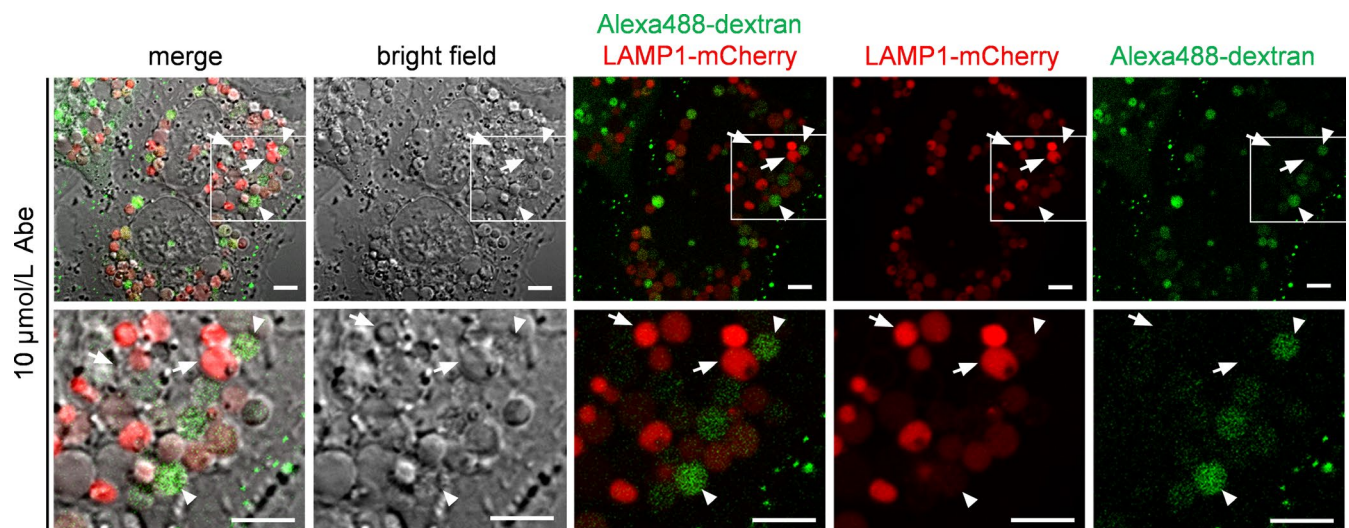
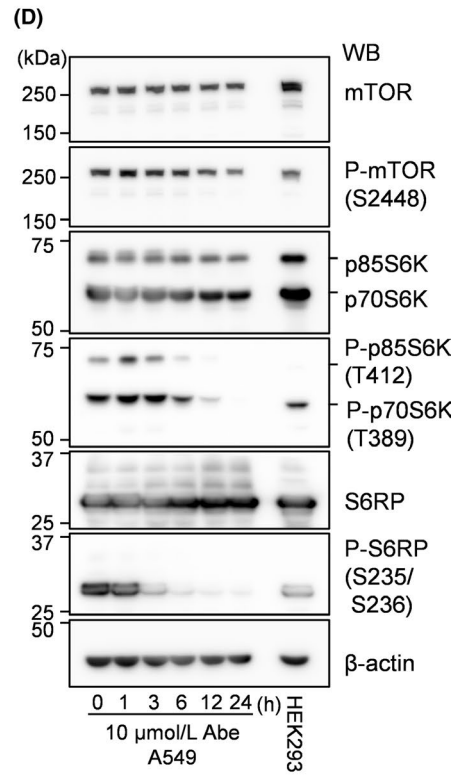
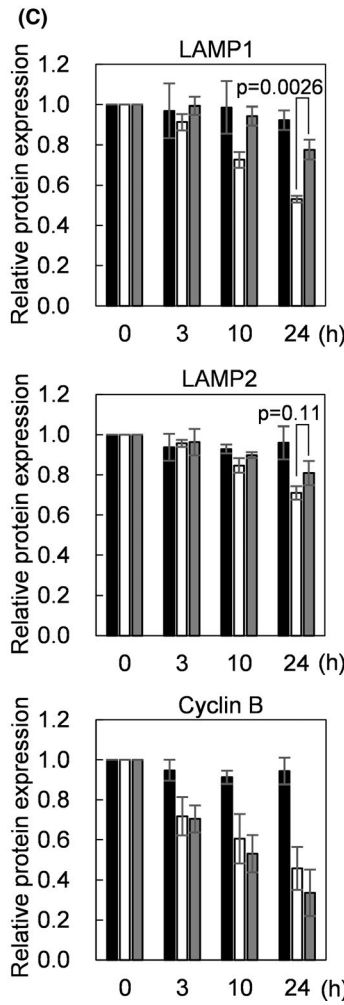
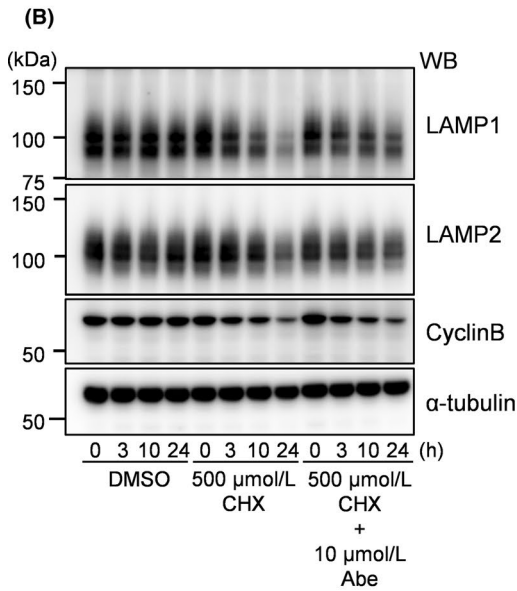
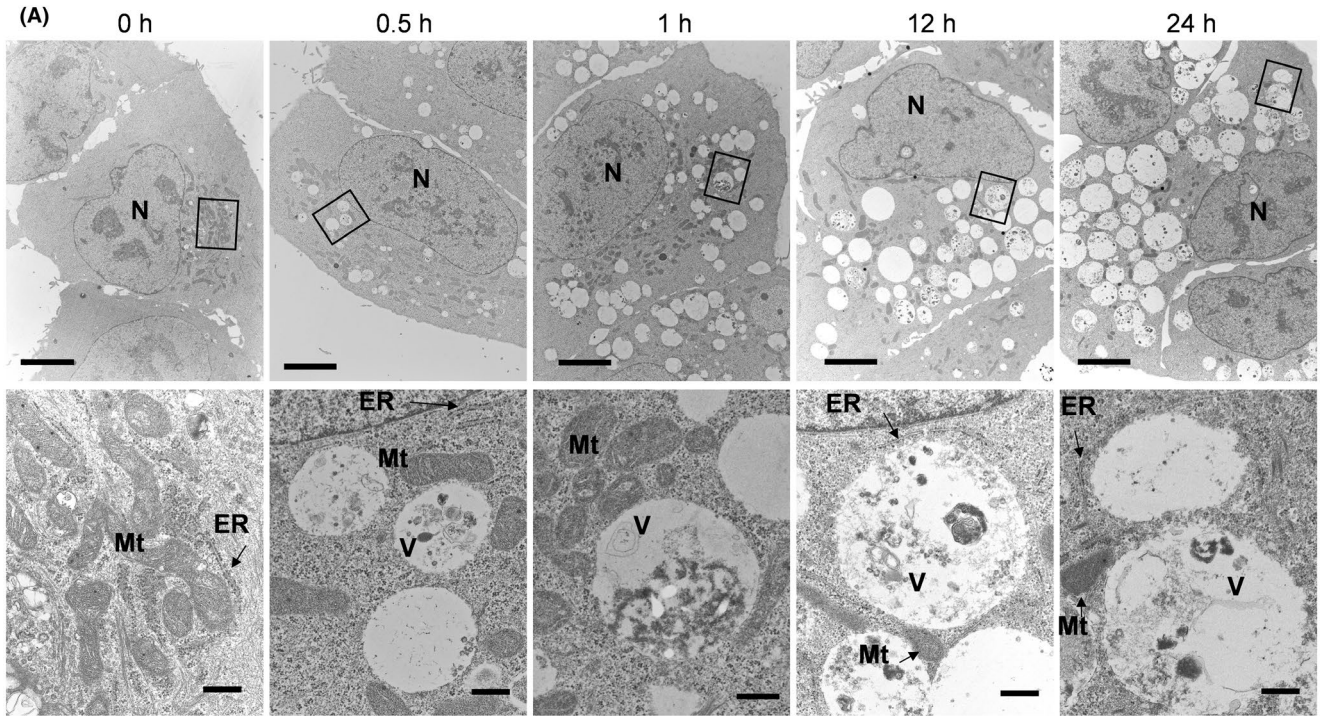


FIGURE 6 Analysis of relationship between endosomes and cytoplasmic vacuoles induced by abemaciclib. A549/LAMP1-mCherry cells were cultured with 50 $\mu\text{mol/L}$ fluorescent dextran and 10 $\mu\text{mol/L}$ Abe for 8 h. Observation was performed after dextran was removed. Arrows indicate LAMP1-mCherry localizing lysosome, and arrowheads indicate Alexa488-dextran localizing endosomes. Bottom represents high-magnification images of the area indicated by open squares. Scale bars: 5 μm . The images not treated with Abe are presented as Figure S6C



■ DMSO
 □ CHX
 ■ CHX+Abe

FIGURE 7 Analyses of lysosomal dysfunctions treated by abemaciclib. A, A549 cells were treated with 10 $\mu\text{mol/L}$ Abe for the indicated time periods. After fixation, the cells were observed by transmission electron microscopy. Bottom images represent higher magnifications of the areas indicated by open squares in the upper row. Mt: mitochondrion, N: nucleus, V: vacuole. Scale bars in upper row: 5 μm , Scale bars in lower row: 500 nm. B, A549 cells were treated with 500 $\mu\text{mol/L}$ CHX in the presence or absence of 10 $\mu\text{mol/L}$ Abe for the indicated time periods. Cellular proteins were extracted and analyzed by western blotting using the indicated antibodies. C, Signal intensity of each band of (B) was quantified using CS Analyzer 4 software, normalized by α -tubulin. In each condition, signal intensity at 0 h was defined as 1. Data represent average values from 3 independent experiments. *P*-values of *t* tests are indicated. D, A549 cells were treated with 10 $\mu\text{mol/L}$ Abe for the indicated time periods. Cellular proteins were extracted and analyzed by western blotting using the indicated antibodies. S6K: S6 kinase; S6RP: S6 ribosomal protein. "P-" means "phosphorylated." As a control for western blotting, cell lysate of HEK293 cells was used

recognized to induce many types of cell death.⁴⁷ Cationic materials, such as gold nanoparticle, have been shown to induce the rupture of lysosomal compartments through the lysosomal swelling, named proton sponge effect, and subsequently induce apoptosis via the massive calcium influx into the cells caused by lysosomal rupture.⁴⁹ In our data, time-lapse imaging revealed that during a 24-h exposure to abemaciclib, most expanding lysosomes were unruptured (Movies S1 and S2), and immunostaining of galectin-3 exhibited that LMP induction was modest and limited (Figure S7). The intracellular calcium concentration was increased by abemaciclib, while the cells treated with LLOMe with potent LMP inducibility resulted in a small increment (Figure S8). Therefore, although the increased intracellular calcium concentration by abemaciclib might be involved in cell-death execution, it is unlikely that the increment of the calcium concentration is due to LMP. Thus, the cell-death phenotype induced by abemaciclib appears to be distinct from that observed with cationic materials.⁴⁹ However, the cytoplasmic release of lysosomal

hydrolyzes including cathepsins might be involved in cell death execution even though most expanding lysosomes were unruptured.

Our data also suggest that the target of abemaciclib relevant to vacuole formation is V-ATPase rather than CDK4/6 (Figure 4D,E). All 3 CDK4/6 inhibitors inhibited Rb phosphorylation (Figure S1). However, it was noteworthy that only abemaciclib induced prominent cytoplasmic vacuolization derived from lysosome along with prominent cytotoxicity (Figure 2A). This suggests that, unlike other CDK4/6 inhibitors, only abemaciclib acts on the V-ATPase that may cause all unique phenotypes shown here. Brown et al reported accelerated induction of autophagy in cells lacking cyclin D1 due to either gene mutation or knockdown.²⁹ By contrast, in this study, abemaciclib did inhibit autophagic flux (Figure 3). This observation also supports the idea that a target or targets other than CDK4/6 contribute to lysosomal dysfunction. Several previous studies reported induction of autophagy in response to CDK4/6 inhibitors.^{29-34,50} In this study, we sequentially monitored autophagic flux using fluorescence probe³⁷; this analysis revealed that all 3 CDK4/6 inhibitors tested inhibited autophagic flux at early time points. Only palbociclib yielded a biphasic curve in the GFP/mCherry ratio over 24-h treatment (Figure 3). Therefore, the controversy regarding induction vs inhibition of autophagy might be due to differences between studies in exposure time or cell type. However, abemaciclib treatment caused accumulation of mCherry-GFP-LC3 dots (Figure 5A), as well as GFP-LC3 dots, as in the case of bafilomycin A1 (Figure 3D), indicating that inhibition might occur at a late stage of autophagic processing, eg, autolysosome formation. In addition, transmission electron microscopy revealed that lysosomal vacuoles contained undigested debris, also supporting the idea of lysosomal dysfunction (Figure 7A). Furthermore, CHX chase assay revealed that lysosomal membrane protein degradation was blocked by abemaciclib (Figure 7B,C), suggesting disruption of lysosomal turnover caused by dysfunction. In addition to its role in cellular catabolism, the lysosome functions as a platform for nutrient sensing and metabolic signal transduction through the mTORC1 protein kinase complex. Signaling from the lysosomal surface, mTORC1 transduces downstream anabolic pathways, resulting in promotion of cell growth; therefore, abnormal mTORC1 nutrient sensing could cause cancer cell proliferation.^{20,45,46} In this study, mTORC1 activity was inhibited by abemaciclib treatment (Figure 7D), and cytoplasmic vacuole formation and cell death induced by abemaciclib were independent of the autophagic catabolic process, implying that inhibition of anabolic signaling from

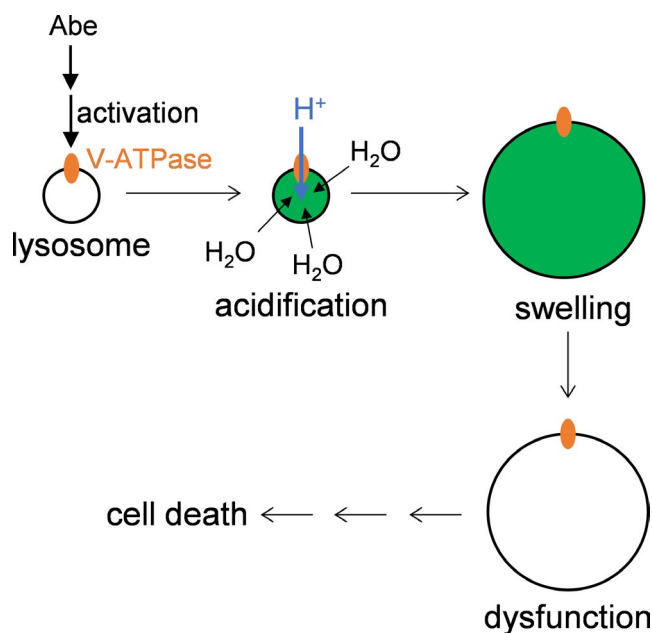


FIGURE 8 Model of lysosomal expansion in response to abemaciclib treatment. Abe might directly or indirectly target V-ATPase, which activates H⁺ transport, leading to lysosomal acidification followed by H₂O influx. This induces lysosomal swelling, as well as lysosomal dysfunction, and ultimately results in induction of cell death via a novel molecular mechanism

the lysosomal mTORC1 complex might be related to these cellular phenotypes of abemaciclib.

In conclusion, we showed that abemaciclib induces an atypical cell-death phenotype characterized by lysosomal vacuolation. Because swelling of lysosomes appears to be closely linked with the more potent cytotoxic effect of abemaciclib relative to palbociclib and ribociclib, future studies should seek to identify the target of abemaciclib responsible for lysosomal swelling, as well as the factors involved in execution of this unique form of lysosome-related cell death. Such knowledge would further clarify the indications and usage of combination therapy for abemaciclib in cancer therapy.

ACKNOWLEDGMENTS

We thank Professor Noboru Mizushima (The University of Tokyo, Graduate School and Faculty of Medicine, Tokyo, Japan) for the kind gift of the GFP-LC3-RFP-LC3ΔG plasmid. We also thank Dr Akihisa Abe, Dr Kana Miyahara, Dr Yu Saito, Ms Ayako Hirota, Ms Yumiko Yamada, Ms Mayumi Tokuhisa, and Ms Jun Takemura for their technical assistance, helpful advice, and fruitful discussions. This study was supported by the MEXT-supported program of the Strategic Research Foundation at Private Universities (S1411011, 2014-2018) from the Ministry of Education, Culture, Sports, Science and Technology of Japan (to KM); and by JSPS KAKENHI (JP18K15031) (to HH).

CONFLICT OF INTEREST

Authors declare no conflicts of interest for this article.

ORCID

Hirotsugu Hino  <https://orcid.org/0000-0001-7560-2442>

Keisuke Miyazawa  <https://orcid.org/0000-0002-8435-1304>

REFERENCES

- Malumbres M, Barbacid M. To cycle or not to cycle: a critical decision in cancer. *Nat Rev Cancer*. 2001;1:222-231.
- Malumbres M, Barbacid M. Cell cycle, CDKs and cancer: a changing paradigm. *Nat Rev Cancer*. 2009;9:153-166.
- Fry DW, Harvey PJ, Keller PR, et al. Specific inhibition of cyclin-dependent kinase 4/6 by PD 0332991 and associated antitumor activity in human tumor xenografts. *Mol Cancer Ther*. 2004;3:1427-1438.
- Toogood PL, Harvey PJ, Repine JT, et al. Discovery of a potent and selective inhibitor of cyclin-dependent kinase 4/6. *J Med Chem*. 2005;48:2388-2406.
- Rader J, Russell MR, Hart LS, et al. Dual CDK4/CDK6 inhibition induces cell-cycle arrest and senescence in neuroblastoma. *Clin Cancer Res*. 2013;19:6173-6182.
- Tate SC, Cai S, Ajamie RT, et al. Semi-mechanistic pharmacokinetic/pharmacodynamic modeling of the antitumor activity of LY2835219, a new cyclin-dependent kinase 4/6 inhibitor, in mice bearing human tumor xenografts. *Clin Cancer Res*. 2014;20:3763-3774.
- Gelbert LM, Cai S, Lin X, et al. Preclinical characterization of the CDK4/6 inhibitor LY2835219: in-vivo cell cycle-dependent/independent anti-tumor activities alone/in combination with gemcitabine. *Invest New Drugs*. 2014;32:825-837.
- Asghar U, Witkiewicz AK, Turner NC, Knudsen ES. The history and future of targeting cyclin-dependent kinases in cancer therapy. *Nat Rev Drug Discov*. 2015;14:130-146.
- Fernandes MT, Adashek JJ, Barreto CMN, et al. A paradigm shift for the treatment of hormone receptor-positive, human epidermal growth factor receptor 2-negative (HR+/HER2-) advanced breast cancer: a review of CDK inhibitors. *Drugs Context*. 2018;7:212555.
- Dickson MA. Molecular pathways: CDK4 inhibitors for cancer therapy. *Clin Cancer Res*. 2014;20:3379-3383.
- Luzio JP, Pryor PR, Bright NA. Lysosomes: fusion and function. *Nat Rev Mol Cell Biol*. 2007;8:622-632.
- Eskelinen EL, Saftig P. Autophagy: a lysosomal degradation pathway with a central role in health and disease. *Biochim Biophys Acta*. 2009;1793:664-673.
- Saftig P, Klumperman J. Lysosome biogenesis and lysosomal membrane proteins: trafficking meets function. *Nat Rev Mol Cell Biol*. 2009;10:623-635.
- Lübke T, Lobel P, Sleat DE. Proteomics of the lysosome. *Biochim Biophys Acta*. 2009;1793:625-635.
- Mindell JA. Lysosomal acidification mechanisms. *Annu Rev Physiol*. 2012;74:69-86.
- Zschenker O, Illies T, Ameis D. Overexpression of lysosomal acid lipase and other proteins in atherosclerosis. *J Biochem*. 2006;140:23-38.
- Ballabio A, Gieselmann V. Lysosomal disorders: from storage to cellular damage. *Biochim Biophys Acta*. 2009;1793:684-696.
- Lee JH, Yu WH, Kumar A, et al. Lysosomal proteolysis and autophagy require presenilin 1 and are disrupted by Alzheimer-related PS1 mutations. *Cell*. 2010;141:1146-1158.
- Platt FM, Boland B, van der Spoel AC. The cell biology of disease: lysosomal storage disorders: the cellular impact of lysosomal dysfunction. *J Cell Biol*. 2012;199:723-734.
- Bar-Peled L, Chantranupong L, Cherniack AD, et al. A tumor suppressor complex with GAP activity for the Rag GTPases that signal amino acid sufficiency to mTORC1. *Science*. 2013;340:1100-1106.
- White E. The role for autophagy in cancer. *J Clin Invest*. 2015;125:42-46.
- Perera RM, Bardeesy N. Pancreatic cancer metabolism: breaking it down to build it back up. *Cancer Discov*. 2015;5:1247-1261.
- Wyant GA, Abu-Remaileh M, Wolfson RL, et al. mTORC1 activator SLC38A9 is required to efflux essential amino acids from lysosomes and use protein as a nutrient. *Cell*. 2017;171(642-654):e612.
- Li J, McQuade T, Siemer AB, et al. The RIP1/RIP3 necrosome forms a functional amyloid signaling complex required for programmed necrosis. *Cell*. 2012;150:339-350.
- Sun L, Wang H, Wang Z, et al. Mixed lineage kinase domain-like protein mediates necrosis signaling downstream of RIP3 kinase. *Cell*. 2012;148:213-227.
- Weinlich R, Oberst A, Beere HM, Green DR. Necroptosis in development, inflammation and disease. *Nat Rev Mol Cell Biol*. 2017;18:127-136.
- Zhang Y, Su SS, Zhao S, et al. RIP1 autophosphorylation is promoted by mitochondrial ROS and is essential for RIP3 recruitment into necrosome. *Nat Commun*. 2017;8:14329.
- Oyadomari S, Mori M. Roles of CHOP/GADD153 in endoplasmic reticulum stress. *Cell Death Differ*. 2004;11:381-389.
- Brown NE, Jeselsohn R, Bihani T, et al. Cyclin D1 activity regulates autophagy and senescence in the mammary epithelium. *Cancer Res*. 2012;72:6477-6489.
- Capparelli C, Chiavarina B, Whitaker-Menezes D, et al. CDK inhibitors (p16/p19/p21) induce senescence and autophagy in cancer-associated fibroblasts, "fueling" tumor growth via paracrine

- interactions, without an increase in neo-angiogenesis. *Cell Cycle*. 2012;11:3599-3610.
31. Sumi NJ, Kuenzi BM, Knezevic CE, Remsing Rix LL, Rix U. Chemoproteomics reveals novel protein and lipid kinase targets of clinical CDK4/6 inhibitors in lung cancer. *ACS Chem Biol*. 2015;10:2680-2686.
 32. Acevedo M, Vernier M, Mignacca L, et al. A CDK4/6-dependent epigenetic mechanism protects cancer cells from PML-induced senescence. *Cancer Res*. 2016;76:3252-3264.
 33. Hsieh FS, Chen YL, Hung MH, et al. Palbociclib induces activation of AMPK and inhibits hepatocellular carcinoma in a CDK4/6-independent manner. *Mol Oncol*. 2017;11:1035-1049.
 34. Vijayaraghavan S, Karakas C, Doostan I, et al. CDK4/6 and autophagy inhibitors synergistically induce senescence in Rb positive cytoplasmic cyclin E negative cancers. *Nat Commun*. 2017;8:15916.
 35. Small J, Washburn E, Millington K, Zhu J, Holder SL. The addition of abemaciclib to sunitinib induces regression of renal cell carcinoma xenograft tumors. *Oncotarget*. 2017;8:95116-95134.
 36. Tanaka H, Hino H, Moriya S, et al. Comparison of autophagy inducibility in various tyrosine kinase inhibitors and their enhanced cytotoxicity via inhibition of autophagy in cancer cells in combined treatment with azithromycin. *Biochem Biophys Res*. 2020;22:100750.
 37. Kaizuka T, Morishita H, Hama Y, et al. An autophagic flux probe that releases an internal control. *Mol Cell*. 2016;64:835-849.
 38. Kondo Y, Kanzawa T, Sawaya R, Kondo S. The role of autophagy in cancer development and response to therapy. *Nat Rev Cancer*. 2005;5:726-734.
 39. Swanson JA, Watts C. Macropinocytosis. *Trends Cell Biol*. 1995;5:424-428.
 40. Kerr MC, Teasdale RD. Defining macropinocytosis. *Traffic*. 2009;10:364-371.
 41. Wang JT, Teasdale RD, Liebl D. Macropinosome quantitation assay. *MethodsX*. 2014;1:36-41.
 42. Overmeyer JH, Young AM, Bhanot H, Maltese WA. A chalcone-related small molecule that induces methuosis, a novel form of non-apoptotic cell death, in glioblastoma cells. *Mol Cancer*. 2011;10:69.
 43. Maltese WA, Overmeyer JH. Methuosis: nonapoptotic cell death associated with vacuolization of macropinosome and endosome compartments. *Am J Pathol*. 2014;184:1630-1642.
 44. Maltese WA, Overmeyer JH. Non-apoptotic cell death associated with perturbations of macropinocytosis. *Front Physiol*. 2015;6:38.
 45. Saxton RA, Sabatini DM. mTOR Signaling in Growth, Metabolism, and Disease. *Cell*. 2017;169:361-371.
 46. Lawrence RE, Zoncu R. The lysosome as a cellular centre for signalling, metabolism and quality control. *Nat Cell Biol*. 2019;21:133-142.
 47. Wang F, Gómez-Sintes R, Boya P. Lysosomal membrane permeabilization and cell death. *Traffic*. 2018;19:918-931.
 48. Maejima I, Takahashi A, Omori H, et al. Autophagy sequesters damaged lysosomes to control lysosomal biogenesis and kidney injury. *EMBO J*. 2013;32:2336-2347.
 49. Lee DU, Park JY, Kwon S, Kim YH, Khang D, Hong JH. Apoptotic lysosomal proton sponge effect in tumor tissue by cationic gold nanorods. *Nanoscale*. 2019;11:19980-19993.
 50. Iriyama N, Hino H, Moriya S, et al. The cyclin-dependent kinase 4/6 inhibitor, abemaciclib, exerts dose-dependent cytostatic and cytotoxic effects and induces autophagy in multiple myeloma cells. *Leuk Lymphoma*. 2018;59:1439-1450.

SUPPORTING INFORMATION

Additional supporting information may be found online in the Supporting Information section.

How to cite this article: Hino H, Iriyama N, Kokuba H, et al. Abemaciclib induces atypical cell death in cancer cells characterized by formation of cytoplasmic vacuoles derived from lysosomes. *Cancer Sci*. 2020;111:2132-2145. <https://doi.org/10.1111/cas.14419>